Numerical Investigation on Three-dimensional Shock Train Structures in Rectangular Isolators

F. Gnani,* H. Zare-Behtash, C. White, and K. Kontis

University of Glasgow, School of Engineering, Glasgow G12 8QQ, UK

Abstract

The understanding of the formation of shock trains in high-speed engines is vital for the improvement of engine design. The formation of these flow structures in a narrow duct, driven by the presence of the viscous effects on the walls, is an extremely complex process that is not fully understood. This investigation demonstrates the high sensitivity of the shock train to the solving equations. The establishment of the shock train in the duct mainly depends on the way that the boundary layer develops on the walls. The k-ω Wilcox model confirms to be the most suitable to accurately reproduce the subtle features close to the solid boundary. The assumption of two-dimensional flow is not completely accurate for describing internal flows where the three-dimensional effects from the shock wave/boundary layer interactions cannot be neglected. The centreline flow properties show that the first shock wave has the same strength in the two- and three-dimensional cases. However, in the three-dimensional case the thinner boundary layer behind the leading shock allows the flow to expand more in the subsonic region causing a stronger deceleration of the flow behind the first shock.

* f.gnani.1@research.gla.ac.uk

I. NOMENCLATURE

D_{eq}	Equivalent duct diameter $[m]$
H	Test section height $[m]$
L	Test section length $[m]$
M	Mach number
P	Pressure $[Pa]$
T	Temperature $[K]$
t	Time $[s]$
U	Component i of the velocity vector $[m/s]$
W	Test section width $[m]$
x	Streamwise component of the position vector $[m]$
δ	Boundary layer thickness $[mm]$

Subscript

b	Back-pressure
0	Total condition

II. INTRODUCTION

During the flight of a ramjet or a scramjet, the low-density air enters via the engine inlet, where it is compressed through an extremely complex mechanism before reaching the combustor. Between the inlet and the combustor, a nearly parallel duct, called an isolator, is placed to prevent the interaction of the flow at the inlet with that inside the combustion chamber.[1] The combustion of fuel causes a rapid pressure rise in the combustion chamber and the formation of a shock structure inside the isolator results in different conditions upstream and downstream of the flow passage. This flow structure, composed of a series of shock waves, is called a shock train. The ability to accurately predict and control such a shock wave structure would provide a means to enhance the performance of flow devices operating at high speeds such as ramjets and scramjets, the engine efficiency, or the mixing of fuel injected from the combustor walls.[2] Other relevant applications characterised by the presence of shock trains include supersonic compressors, ejectors, and wind-tunnel diffusers.[3]

The shock train system has demonstrated to be largely dependant on the geometry and the flow conditions at the two extremities of the duct.[4,5] In particular, the ratio of boundary layer thickness to duct equivalent hydraulic diameter, δ/D_{eq}, also referred to as flow confinement, is one of the leading variables that determines the configuration of the shock train.[6–9] Morgan et al.[10] found that the local flow blockage is more important than the total pressure loss in locating the initial shock within an isolator. Weiss et al.[11] confirmed that the confinement level and Mach number are the dominant variables which characterise the position and length of the shock train, whereas the Reynolds number has a much smaller effect.

Figure 1 schematically illustrates the coupling between the shock train and the boundary layer for inflow Mach numbers greater than 1.5. The flow enters the inlet at supersonic speeds and is decelerated to subsonic velocity behind the first normal shock wave, NSW, in the core flow. The pressure rise is transmitted upstream through the boundary layer region, causing a thickening of the boundary layer itself. The growth of the boundary layer deflects the streamline forming an oblique shock, FOS. Since the flow remains supersonic behind the front oblique shock, a rear oblique shock wave, ROS, forms behind it. The two oblique shocks converge into the triple point, TP, and combine with the initial normal shock into a λ shock structure, λS. At the point of bifurcation, a shear layer, SL, develops, as it can be observed in the form of slip lines. In the region confined between the slip lines, the stronger deceleration through the normal shock produces a misalignment of the flow velocity with the outer parts where the flow passes through the two oblique shocks. The thickening of the boundary layer reduces the effective area of the core flow, so that the subsonic flow behind the rear oblique shock wave, ROS, is accelerated again to supersonic velocity. At this point the supersonic flow interacts with the thick boundary layer and the same process is repeated several times up to a terminal shock after which the flow is subsonic in the entire cross section.

The numerous variables which affect the shock train configuration make a comprehensive analysis of the flow field extremely difficult. Some flow measurements in shock trains cannot be experimentally obtained and key mechanisms, such as the interaction between three-dimensional shock waves and recirculation zones, are too complex to be analysed and explained by experiments alone.[12,13] These limitations have led industry towards an increasing use of computational analysis to estimate the flow physics and to design flow devices with adequate performance.[14,15]

The intrinsic problem of numerical methods is that the domain of interest must be divided into cells where a chosen numerical method is applied to solve differential equations, introducing an approximation that differs from the exact solution. The Navier-Stokes (NS) equations are widely employed because they allow the simultaneous solving of the viscous and inviscid flow fields. However, computations which include the interaction between shock waves and turbulence are highly sensitive to the turbulence closure model.[8,16] The shear stress transport model (SST) was successfully used by Saha et al.[17] to predict the wall pressure in an intake with freestream Mach number from 3 to 8, but the numerical simulation performed by Gawehn[18] strongly deviated from the experimental findings. By using the Reynolds stress transport models (RSM) Mousavi et al.[19] successfully predicted the position and shape of the shock train in a convergent-divergent nozzle. Sun et al.[20] obtained good agreement with the experimental data using the algebraic Baldwin-Lomax turbulence model with only one value of the tested back-pressures. The reason of the limited accuracy of the algebraic turbulence model is the Boussinesq approximation, which prevents its use in separated flows.[21–24] Although Chan et al.[14] demonstrated that the k-ω Wilcox model is suitable for supersonic and hypersonic aerothermodynamic applications, at the NASA Langley Research Center, all the models used by Baurle et al.[25] failed to accurately predict the shape and extent of the separated flow region caused by the shock wave/boundary layer interactions in a scramjet isolator.

Most studies have concentrated on two-dimensional simulations[13,26] even though an adequate description of a three-dimensional flow with a two-dimensional model is unreasonable.[27] Three-dimensional investigations provide more accurate insight into the effect of the four walls surrounding rectangular ducts on the complex characteristics of the shock train.[28] To reduce computational time, Sridhar et al.[29] used only one-quarter of the actual duct as computational domain consequently, the results displayed a symmetrical flow field, in contrast with the experimental findings.

Additionally, research on high-speed isolators has mainly focused on cylindrical ducts, and only recently on rectangular cross-sections. This choice is due to the fact that the axisymmetric configuration minimises the three-dimensional effects from the shock wave/boundary layer interactions encountered in rectangular channels.[30] The numerical and experimental results by Kawatsu et al.[31] reported that in rectangular ducts, the boundary layer separation occurs only near the corners of the duct but not at the centre plane of the test section, as it is observed with schlieren photography. Although Billig et al.[32] stated that since the trend of the pressure rise for cylindrical and rectangular cross-sections is quite similar then the shock train characteristics may also be similar, no similarity law linking different cross-sectional geometries have been reported. In contrast, differences have been highlighted by Lin et al.[33] observing that, compared to rounded cross-sectional area ducts, in the rectangular configuration the pressure profile of the shock train initially rises steeply, reaches a maximum value early, and drops quickly at the isolator exit. Also, the maximum pressure rise is smaller, independent of the Mach number. These differences were attributed to the fact that in the rectangular duct, the larger cross-sectional perimeter and the presence of the four corners lead to an increased cross-sectional area of the duct covered by the boundary layer, thus reducing the effective free-stream area. On the other hand, for the same Mach number, the leading edge of the shock train was detected to be roughly at the same axial position inside the isolator for both circular and rectangular cross-sections.

The present study analyses the sensitivity to the variables that influence the characteristics of the shock system which establish in a long duct. The effects of the choice of the turbulence model and the use of a three-dimensional domain are investigated.

III. NUMERICAL AND PHYSICAL SETUP

To validate the numerical approach, the Mach 2 shock train experimentally studied by Sun et al.[13,20] in a square duct was replicated. The boundary and geometrical conditions are reported in Table I. The cross section and length of the test section are $80 \times 80\ mm^2$ and 1500

$\boldsymbol{M}$	$\boldsymbol{T_0[K]}$	$\boldsymbol{P_0[kPa]}$	$\boldsymbol{P_b[kPa]}$	$\boldsymbol{H[mm]}$	$\boldsymbol{W[mm]}$	$\boldsymbol{L[mm]}$	$\boldsymbol{\delta/D_{eq}}$
2	300	196	92.2	80	80	880	0.25

Table I. Boundary and geometry conditions of the computational domain of the validation model.[20] The subscript 0 refers to the total condition and P_b is the back-pressure.

mm, with a length to equivalent diameter ratio L/D_{eq} of 18.75. Along with experiments, Sun et al.[13,20] performed a numerical investigation with a computational domain length of 11 times the height starting from L/D_{eq}= 7. Since the effect of the flow confinement, δ/D_{eq}, at the inlet of the computational domain plays a fundamental role in the location of the shock train, to match the experimental conditions of δ/D_{eq}= 0.25, Sun et al.[20] imposed a velocity profile given by the 1/7-power law at the inlet.

The numerical simulations were carried out by solving the two-dimensional coupled implicit Reynolds-averaged Navier-Stokes (RANS) equations in STAR-CCM+[34]. In real supersonic air-breathing engines, the shock train is inherently unsteady due to the combustion instabilities.[35] However, longitudinal fluctuations around the averaged position are small and can be assessed in a steady manner. The k-ω Wilcox turbulence model was used in most cases. This model is able to reproduce subtle features close to the solid boundary and is more accurate for two-dimensional boundary layers with both favourable and adverse pressure gradients, and in the presence of separation induced by the interaction with a shock wave.[36]

The RANS equations are discretised using the cell-centred finite volume method. The inviscid and viscous fluxes are evaluated using respectively the Liou's AUSM+ flux-vector splitting scheme based on the upwind concept and the second-order central differences.

The working fluid is approximated as an ideal gas. The viscosity and thermal conductivity are evaluated using Sutherland's law. Adiabatic and no-slip boundary conditions are imposed on the walls along the duct. Initial conditions are set with an inviscid normal shock at the exit of the computational domain. At the outlet boundary the flow variables except pressure are extrapolated from the adjacent cell value using reconstruction gradients. The back-pressure was determined from the experimental results to be approximately P_b= 92.2 kPa and assumed constant at the exit plane.

The static pressure and Mach number distributions along the duct obtained by Sun et al.[13] through numerical simulations and experiments are shown in Figure 2. Two values of the back-pressure, P_b= 92.2 kPa (case A) and 96.6 kPa (case B), are compared for an inlet Mach number of 2. It can be observed that the experimental pressure data at the wall of case B are well replicated with the numerical simulations. For case A, although the location of the first shock wave matches the experimental findings, the pressure distribution is not well-resolved. The poor accuracy of the numerical results obtained by Sun et al.[13,20] due to the use of an inadequate turbulence model to describe separated flows is an important aspect to take into account when the discrepancies with the current numerical code are analysed. Additionally, the only experimental data available are from the pressure tapping at the wall, whereas pressure and Mach number distributions at the duct centreline are obtained with computation only. Therefore, only the wall pressure distributions are considered reliable to make comparisons.

The computational domain used in the current study is formed of a rectangular block. Due to the symmetry of the problem, half of the region of the flow field is computed in the two-dimensional case, and one quarter in the three-dimensional case. The mesh is composed of structured quadrilateral cells and the grid points are clustered towards the wall to resolve the behaviour of the boundary layer. Refinements are necessary in the regions where the gradients are known to be relevant and the thickness of the closest cell to the wall is important for the accuracy of the results. Figure 3 shows the structure of the numerical grid employed, where $y/D_{eq}= 0$ corresponds to the wall and $y/D_{eq}= 0.5$ is the centreline of the duct.

IV. RESULTS AND DISCUSSION

A. Two-dimensional Grid Convergence

In a narrow channel, typical of this kind of flows, the ratio of the flow confinement ahead of the shock train to the duct height plays a fundamental role on the location and length of the shock train. Without a boundary layer at the inlet of the computational domain the shock train would begin further downstream in the duct, in agreement with Huang et al.[37] However, the viscous effects near the wall reduce the flow speed and also the effective area of the duct. This leads to a high sensitivity of the shock train to the length of the computational domain. In the results achieved by Sun et al.[13] a portion of duct with length $L/D_{eq}= 11$ was taken to process the data, with the inlet located at δ/D_{eq} equal to approximately 0.25. To replicate the same inlet conditions, an iterative process of mesh refinement and duct length analysis was performed. An initial simulation was run to extract the flow properties at a specific axial location, which are then imposed at the inlet of another simulation as a fixed boundary condition. Figure 4 illustrates that by imposing a boundary layer profile at the inlet of the computational domain the shock train establishes in the same manner as with the case in which the boundary layer naturally develops along the duct walls.

The imposition of the boundary layer at the inlet of the computational domain requires a numerically expensive procedure since two simulations need to be run. Therefore, in the current study the boundary layer was left to develop along the duct wall as it occurs naturally in the experiments by using a computational domain of length L/D_{eq}= 23. This value ensures an inlet Mach number equal to 2 ahead of the shock train and establishes the boundary layer similar to the reference study.[13] Only the portion of the duct with a length 11 times the height was taken to process the data, with the inlet located at δ/D_{eq} equal to approximately 0.25.[20]

Since the quality of the numerical solution mainly depends on the size of the grid cells and their distribution in the computational domain, seven grids, tabulated in Table II, are employed to find the optimal combination between the requirements of adequate accuracy and computational resources. Except for Grid 1, for all the finer grids the value of the wall

Grid	1	2	3	4	5	6	7
N_x	368	921	2454	4601	6134	9200	12268
N_y	62	116	154	276	314	350	452

Table II. Number of cells in different grids.

y^+ is smaller than unity in the entire domain, providing a good resolution of the boundary layer gradients.

The flow properties distributions illustrated in Figure 5 have been shifted by the location of the initial shock wave so that they start at the same axial coordinate. The wall static pressure monotonically increases due to the diffusing effect of the boundary layer. On the other hand, the peaks in the centreline pressure plot identify the individual waves composing the shock train which are gradually damped along the duct. Although the general behaviour of the shock train is similar in the seven cases, as the mesh resolution increases, the shock train moves upstream towards the inlet and increases in length. This is caused by the fact that a coarse mesh fails to adequately resolve the fine structures such as the boundary layer. Fine grids better match the experimental data because the representation of the flow field is more accurate. Since the back-pressure is prescribed as a boundary condition, the pressure at the end of the shock train always converges towards the experimental value. These results agree with all cases in literature despite the contradictory finding by Carroll et al.,[24] who observed that a grid refinement in the transverse direction only causes the shock train to move toward the exit plane.

From Figure 5, as the grid is refined, the difference between two subsequent pressure profiles gradually decreases and the location of the shock train tends to stabilise at a fixed axial coordinate. The difference between Grid 6 and Grid 7 is not significant and the relative error is less than 1.2%. The relative error in the axial coordinate of the shock train between Grid 4 and Grid 7 is approximately 8%. However, Figure 6 show very little changes for grids finer than Grid 4. The difference in the magnitude of the pressure peaks of the first and second shocks, respectively peak 1^{st} shock and peak 2^{nd} shock, and the pressure recovery behind the 1^{st} shock converge towards asymptotic values. The variation in magnitude of the first and second shock between Grid 4 and Grid 7 is less than 0.2%, as it is also evident from the centreline pressure profile, in Figure 5(b). Taking into account both the accuracy of the grid and the computational cost, Grid 6 is used to perform the simulations reported in the present study apart from the three-dimensional case when, due to the large number of cells, Grid 4 is used.

B. Effect of Turbulence Model

The influence of using three different turbulence models, the k-ω Wilcox, k-ω Menter SST, and k-ε realisable, is investigated. As Figure 7 illustrates, compared to the k-ω Wilcox model, the magnitude of the density gradient obtained with the k-ω Menter SST and k-ε realisable models show several differences. From the close up in Figures 8(b) and 8(c) the leading shock wave is not normal at the centre of the duct. The front shock has a χ shape, identified as χS, although in the k-ε case, in Figure 8(c), a slip line, SL, at the centreline is visible. It is interesting to note that in the k-ω Menter SST case, in Figure 8(b), a weak slip line is present just behind the first shock wave. A second shock occurs and is linked to the rear legs of the oblique shocks at the edge of the boundary layer. This latter shock, SN, is normal in a small portion at the centreline of the duct and decelerates the flow to subsonic conditions. The centreline pressure distribution, in Figure 9(a), illustrates that with the k-ω Menter SST the initial pressure rise is not composed of a single peak. The flow passing through the χ shock is decelerated but remains in the supersonic range. The flow is further decelerated to subsonic speeds through the normal shock that corresponds to the steep pressure rise in the first pressure peak.

From the pressure distributions in Figure 9, both the wall and centreline pressure converge to the value of the back-pressure imposed as the boundary condition. The wall pressure in the k-ω Menter SST model is underpredicted, as visible in Figure 9(b). Although the k-ε model locates the shock train several L/D_{eq} downstream in the duct, it predicts the shock train structure more accurately. Compared against the k-ω Wilcox, the spacing between consecutive shocks is quite accurate but the amplitude of the shocks behind the leading shocks is overpredicted and the latter shocks in the shock train structure are very weak. The considerably shorter shock train length may also be a contributing factor. The k-ω Menter SST model predicts a slightly longer shock train but it fails to locate the several shock waves of the shock train system on the axial coordinates. The absence of a normal portion of the leading shock at the centreline contributes to the failure in capturing the subsonic flow following the first shock and consequently the entire structure of the shock train is affected.

The establishment of the shock train in the duct mainly depends on the way the boundary layer develops on the walls, and hence a model capable to accurately reproduce the subtle features close to the solid boundary plays a fundamental role. Although the three turbulence models employed are two-equation models, only the k-ω Wilcox fulfils this requirement. As shown in Figure 5, the k-ω Wilcox closely matches the reference data by Sun et al.[13] of the entire shock train in terms of flow properties, location of the shock train, distance between shocks, and shock strength. There is considerable evidence in the literature that the k-ω model is more computationally robust than the k-ε model for the description of turbulent flows close to a solid boundary.[38] The k-ω Menter SST includes the k-ε model in the far-field through a blending function. This demonstrates the inability of the k-ε to describe the shock train characteristics even in the core flow. On the other hand, the k-ω Wilcox model confirms to be the most suitable for describing the shock train behaviour in internal ducts.

C. Sidewalls Effects

Two-dimensional simulations have the advantage of being efficient since the inclusion of the third dimension costs additional computational time. However, the presence of the sidewalls cannot be neglected when the duct aspect ratio is unity. Grid 4 is used to generate the two-dimensional computational domain. The same grid structure with the addition of the third dimension is applied to the three-dimensional domain. Due to the symmetry of the duct, one quarter of the experimental geometry is simulated in the three-dimensional case with a grid composed of 28 million cells.

As visible from Figure 10 the location of the shock train in the 3D case occurs with an apparent thin boundary layer. In reality, compared to the 2D case, in 3D the shock train occurs further upstream because of the effect of the boundary layer on the side walls and the corners. In the 2D case, the boundary layer develops only on the top and bottom walls of the test section, but in the 3D case the boundary layer on the side walls and the corners is also a contributing factor. Since the duct is of square cross-sectional area, the boundary layer on the side walls affects the flow in the same extent as the top and bottom walls. Consequently, with the inclusion of the boundary layer from all walls, the flow confinement reaches approximately the same value as in the 2D case. This demonstrates that flow confinement plays the greatest role in determining the location of the initial shock, in agreement with the literature.[10,33]

Figure 11 illustrates the numerical schlieren and Mach number contour on different cross sections. The location x_1 identifies the cross section corresponding to the initial pressure rise and the subsequent planes are spaced by $L/D_{eq}= 1$ apart. The cross sections are better displayed in Figure 12. The results show a large separation region at the corners downstream of the leading shock from x_1. The separation extends along the entire duct reducing the core flow. The several shock waves forming the shock train gradually decelerate the core flow so that from approximately x_4 the shocks are very weak. From x_5 the flow structure shows little changes and at approximately x_6 the shock train is terminated.

Figure 13 compares the Mach number and pressure profiles obtained with the 2D and 3D simulations. The plots are shifted for common pressure rise and normalised with the equivalent hydraulic diameter. The pressure profiles, in Figure 13(a), illustrates a small difference between the two cases. The centreline pressure shows that the shape of the shock train is similar in the two cases and, in particular, the first shock wave is captured with the same strength. On the other hand, the flow behind the first shock is decelerated more strongly in 3D, as the deeper trough illustrates. The reason of such a difference is due to the thinner boundary layer behind the leading shock which allows the flow to expand more in the subsonic region. This is believed to cause the non-perfect matching of the subsequent shock waves composing the shock train. As previously explained, the first shock is responsible of determining the shape of the entire shock train structure. The same trend is visible from the Mach number profile in Figure 13(b): since the flow conditions of the incoming flow ahead of the shock train are the same in both cases, the strength of the leading shock matches excellently. However, behind the leading shock the subsequent shocks differ. It emerges that in 3D simulations at the end of the shock train the flow is decelerated to a lower Mach number. The lack of experimental data cannot confirm the real Mach number variation through the shock train. Therefore, taking into account the limitation due to the absence of the sidewall effects, two-dimensional simulations are still useful for the qualitative understanding of the mechanism of formation of the shock train in long ducts.

V. CONCLUSIONS

The formation of a shock train structure in an air-breathing engine prevents the interaction of the flow at the inlet with that inside the combustion chamber guaranteeing that the air entering the combustor is decelerated to lower speeds. The understanding of such a flow structure is vital for the improvement of the design of high-speed engines as well as the development of flow control methodologies.

This investigation on a shock train at inflow Mach number of 2 in a rectangular duct has demonstrated the high sensitivity of the shock train to the solving equations. Since the shock train establishment in the duct is caused by the interaction with the boundary layer, the flow confinement has demonstrated to be the key parameter in determining the shock train properties. A small error in resolving the boundary layer drastically changes the shape of the leading shock, which influences the overall configuration of the shock train.

The difficulties in achieving grid-independent results reflects the characteristic of supersonic flows in long ducts being extremely complicated. The dependence of the shock train on the grid size showed that as the grid is refined the differences between two subsequent grids become gradually smaller leading to the conclusion that a finer grid is expected to give results very close to Grid 7. Of the three turbulence models employed only the k-ω Wilcox closely matches the experimental pressure distribution confirming to be the most suitable for capturing the shock train characteristics.

From the 2D and 3D results the boundary layer thickness influences the shock train shape and location in the duct. At the duct centreline, the flow properties showed that the first shock wave is captured with the same strength. However, in 3D the flow behind the first shock is decelerated more strongly, which then causes a mismatching of the subsequent shock waves composing the shock train. Although two-dimensional simulations qualitatively resolve the mechanism of formation of the shock train in long ducts, the absence of the sidewall effects limits the accuracy. A 3D domain is necessary for the comprehension of the flow physics. However, the solving of the RANS equations with a mesh structure composed of a large number of cells requires an onerous computational power. This study has proven that a compromise between an accurate solution and numerical resources is necessary and that a 2D computation is not adequate to describe the characteristics of shock trains.

[1] Sullins, G., *Experimental Results of Shock Trains in Rectangular Ducts*, AIAA Paper, **92-5103**, 1992.

[2] Yamauchi, H., Choi, B., Kouchi, T., Masuya, G., *Mechanism of Mixing Enhanced by Pseudo-Shock Wave*, AIAA Paper, **2009-25**, 2009.

[3] McLafferty, G., *Theoretical Pressure Recovery Through a Normal Shock in a Duct with Initial Boundary Layer*, Journal of the Aeronautical Sciences, **20(3)**:169-174, 1953.

[4] Curran, E.T., Heiser, W.H., Pratt, D.T., *Fluid phenomena in scramjet combustion systems*, Annual Review of Fluid Mechanics, **28**:323–360, 1996.

[5] Gnani, F., Zare-Behtash, H., Kontis, K., *Pseudo-shock waves and their interactions in high-speed intakes*, Progress in Aerospace Sciences, **82**:36-56, 2016.

[6] Lustwerk, F., *The Influence of Boundary Layer on the 'Normal' Shock Configuration*, Meteor report, **61**, MIT Guided Missiles Program, 1950.

[7] Matsuo, K., Miyazato, Y., Kim, H.D., *Shock train and pseudo-shock phenomena in internal gas flows*, Progress in Aerospace Sciences, **35**:33-100, 1999.

[8] Om, D., Childs, M.E., Viegas, J.R., *Transonic Shock-Wave/Turbulent Boundary-Layer Interactions in a Circular Duct*, AIAA Journal, **23(5)**:707-714, 1985.

[9] Merkli, K., *Pressure Recovery in Rectangular Constant Area Supersonic Diffusers*, AIAA Journal, **14(2)**:168-172, 1976.

[10] Morgan, B., Duraisamy, K., Lele, S.K., *Large-Eddy Simulations of a Normal Shock Train in a Constant-Area Isolator*, AIAA Journal, **52(3)**:539-558, 2014.

[11] Weiss, A., Grzona, A., Olivier, H., *Behavior of shock trains in a diverging duct*, Experiments in Fluids, **49(2)**:355-365, 2010.

[12] Quaatz,J.F., Giglmaier, M., Hickel, S., Adams, N.A., *Large-eddy simulation of a pseudo-shock system in a Laval nozzle*, International Journal of Heat and Fluid Flow, **49**:108-115, 2014.

[13] Sun, L. Sugiyama, H., Mizobata, K., Minato, R., Tojo, A., *Numerical and experimental investigations on Mach 2 and 4 pseudo-shock waves in a square duct*, Transactions of the Japan Society for Aeronautical and Space Sciences, **47(156)**:124-130, 2004.

[14] Chan, W.Y.K., Jacobs, P.A., Mee, D.J., *Suitability of the k-ε turbulence model for scramjet flowfield simulations*, International Journal for Numerical Methods in Fluids, **70(4)**:493-514, 2012.

[15] Hunter, L.G., Tripp, J.M., Howlett, D.G., *Supersonic inlet study using the Navier-Stokes equations*,

Journal of Propulsion and Power, **2(2)**:181-187, 1986.

[16] Nair, M.T., Naresh, K., Saxena, S.K., *Computational analysis of inlet aerodynamics for a hypersonic research vehicle*, Journal of Propulsion and Power, **21(2)**:286-291, 2005.

[17] Saha, S., Chakraborty, D., *Hypersonic intake starting characteristics - A CFD validation study*, Defence Science Journal, **62(3)**:147-152, 2012.

[18] Gawehn, T., Gülhan, A., Al-Hasan, N.S., Schnerr, G.H., *Study on Shock Wave and Turbulent Boundary Layer Interactions in a Square Duct at Mach 2 and 4*, Shock Waves, **20**:297–306, 2010.

[19] Mousavi, S.M., Roohi, E., *Three dimensional investigation of the shock train structure in a convergent-divergent nozzle*, Acta Astronautica, **105(1)**:117-127, 2014.

[20] Sun, L.Q., Sugiyama, H., Mizobata, K., Fukuda, K., *Numerical and Experimental Investigations on the Mach 2 Pseudo-Shock Wave in a Square Duct*, Journal of Visualization, **6(4)**:363-370, 2003.

[21] Wilcox, D.C., *More advanced applications of the multiscale model for turbulent flows*, AIAA paper 88-0220, 1988.

[22] Liou, M.S., Adamson Jr, T.C., *Interaction between a normal shock wave and a turbulent boundary layer at high transonic speeds. Part II: Wall shear stress*, Zeitschrift fr angewandte Mathematik und Physik, **31(2)**:227-246, 1980.

[23] Knight, D.D., *Calculation of Three-Dimensional Shock/Turbulent Boundary-Layer Interaction Generated by Sharp Fin*, AIAA Journal, **23(12)**:1885-1891, 1985.

[24] Carroll, B.F., Lopez-Fernandez, P.A., Dutton, J.C., *Computations and experiments for a multiple normal shock/boundary-layer interaction*, Journal of Propulsion and Power, **9(3)**:405-411, 1993.

[25] Baurle, R.A., Middleton, T.F., Wilson, L.G., *Reynolds-Averaged Turbulence Model Assessment for a Highly Back-Pressured Isolator Flowfield*, JANNAF 45th Combustion Meeting Joint Subcommittee Meeting, Monterey, CA, 2012.

[26] Qin, B., Chang, J., Jiao, X., Bao, W., Yu, D., *Numerical investigation of the impact of asymmetric fuel injection on shock train characteristics*, Acta Astronautica, **105(1)**:66–74, 2014.

[27] Tian, Y., Yang, S., Le, J., *Numerical study on effect of air throttling on combustion mode formation and transition in a dual-mode scramjet combustor*, Aerospace Science and Technology, **52**:173-180, 2016.

[28] Handa, T. Mitsuharu, M.,Matsuo, K., *Three-Dimensional Normal Shock-Wave/Boundary-Layer Interaction in a Rectangular Duct*, AIAA Journal, **43(10)**:2182-2187, 2005.

[29] Sridhar, T., Chandrabose, G., Thanigaiarasu, S., *Numerical Investigation of Geometrical Influence On Isolator Performance*, International Journal on Theoretical and Applied Research in Mechanical Engi-

neering, **2**:7-12, 2013.

[30] Om, D., Childs, M.E., *Multiple Transonic Shock-Wave/Turbulent Boundary-Layer Interactions in a Circular Duct*, AIAA Journal, **23(10)**: 1506-1511, 1985.

[31] Kawatsu, K., Koike, S., Kumasaka, T., Masuya, G., Takita, K., *Pseudo-Shock Wave Produced by Backpressure in Straight and Diverging Rectangular Ducts*, AIAA Paper, **2005-3285**, 2005.

[32] Billig, F.S., Corda, S., Pandolfini, P.P., *Design Techniques for Dual Mode Ram Scramjet Combustors*, AGARD 75th symposium of hypersonic combined cycle propulsion, Madrid, **23**:1-20, 1990.

[33] Lin, K.C., Tam, C.J., Jackson, K.R., Eklund, D.R., Jackson, T.A., *Characterization of Shock Train Structures Inside Constant-Area Isolators of Model Scramjet Combustors*, AIAA Paper **2006-0816**:1442-1452, 2006.

[34] CD-Adapco STAR-CCM+ documentation, 2015.

[35] Oh, J.Y., Ma, F., Hsieh, S.Y., Yang, V., *Interactions Between Shock and Acoustic Waves in a Supersonic Inlet Diffuser*, Journal of Propulsion and Power, **21(3)**:486-495, 2005.

[36] Wilcox, D.C., *Turbulence Modeling for CFD*, DCW Industries, Inc., La Canada, California, 1998.

[37] Huang, W., Wang, Z., Pourkashanian, M., Ma, L., Ingham, D.B., Luo, S., Lei, J., Liu, L., *Numerical investigation on the shock wave transition in a three-dimensional scramjet isolator*, Acta Astronautica, **68(11-12)**:1669-1675, 2011.

[38] Speziale, C.G., Abid, R., Anderson, E.C., *Critical evaluation of two-equation models for near-wall turbulence*, AIAA Journal, **30(2)**:324-331, 1992.

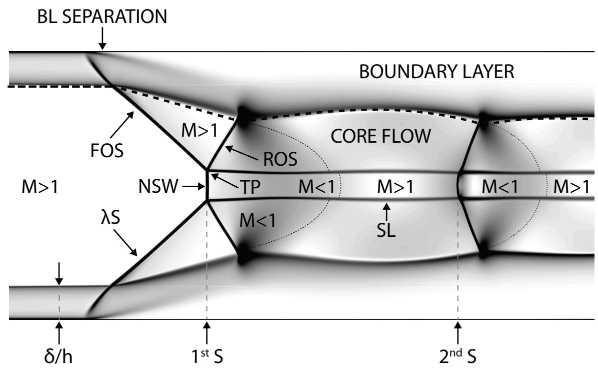

Figure 1. Schematic of the shock wave/boundary layer interaction in shock train obtained with the numerical approach used in the current study.

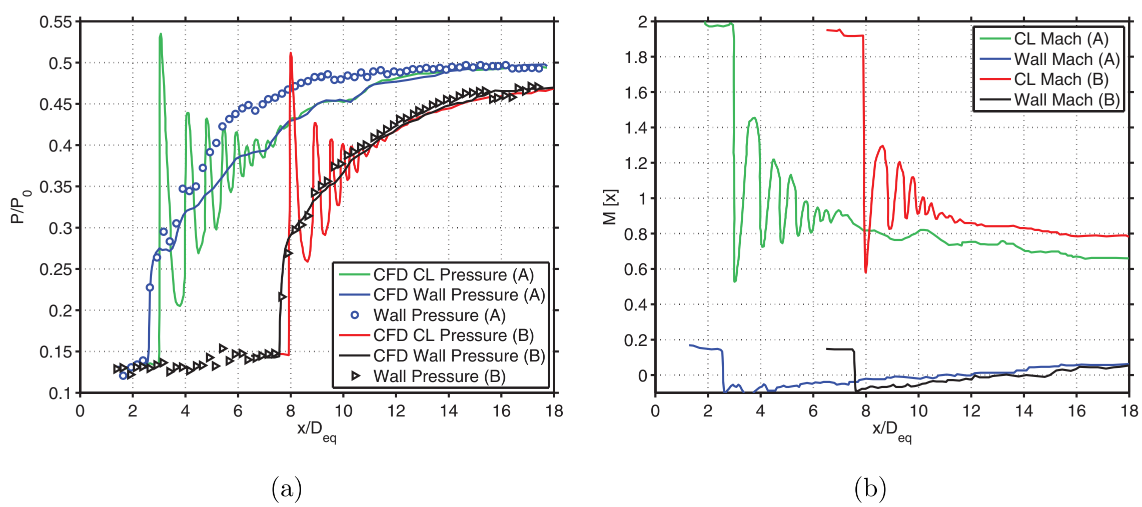

Figure 2. Numerical and experimental static pressure (a) and centreline Mach number (b) distributions obtained by Sun et al.[20] for different back-pressures.

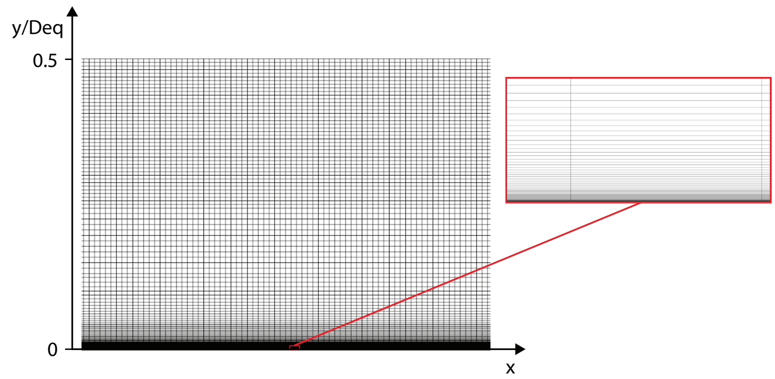

Figure 3. Portion of the half duct numerical grid employed in the 2D computational domain.

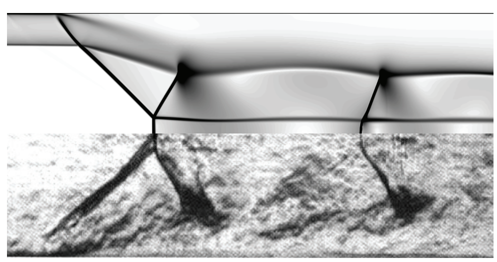

Figure 4. Comparison of schlieren photography from the reference results[13] and the numerical density gradient magnitude obtained with the current numerical approach and .

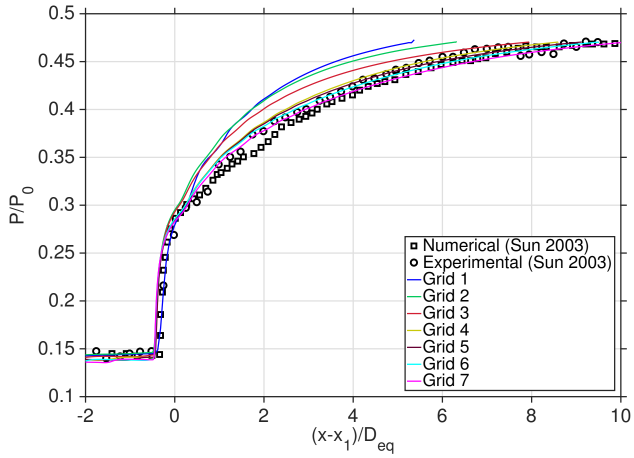

(a)

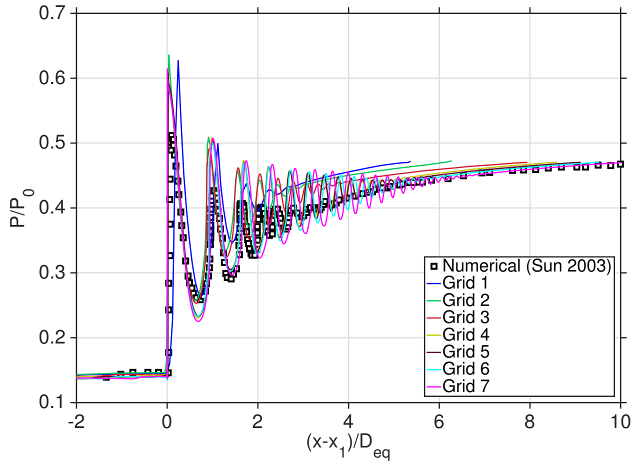

(b)

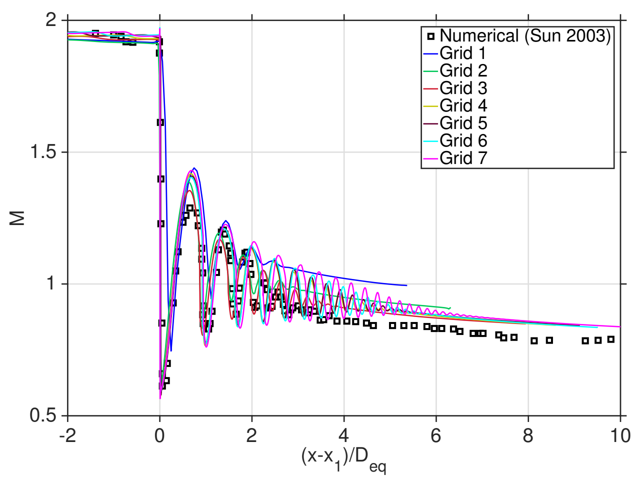

(c)

Figure 5. Effect of grid size on the accuracy of pressure and Mach number distributions. a) Wall static pressure; b) Centreline static pressure; c) Centreline Mach number.

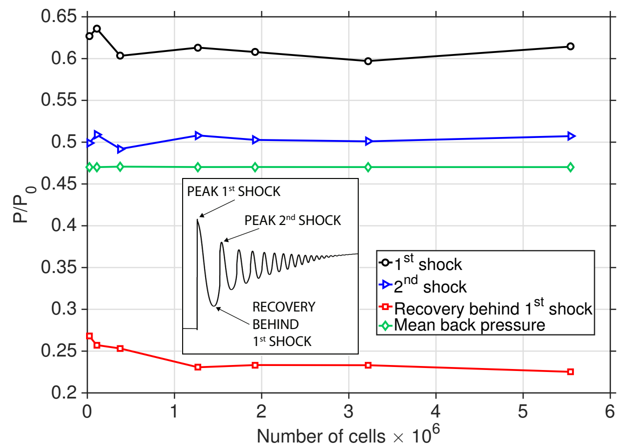

Figure 6. Variation of the value of pressure of different parts of the shock train with grid resolution.

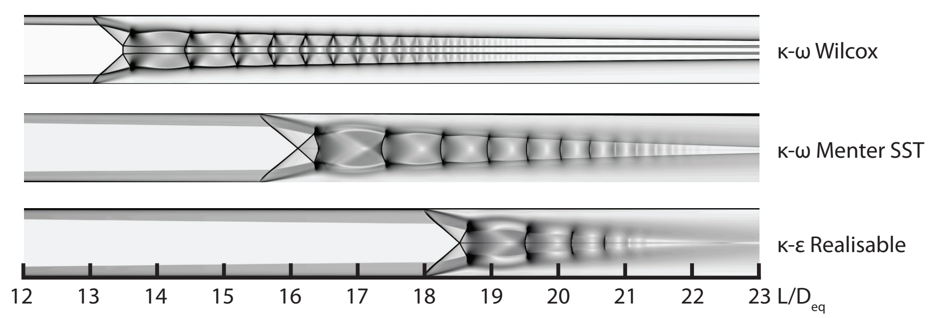

Figure 7. Numerical schlieren with different turbulence model.

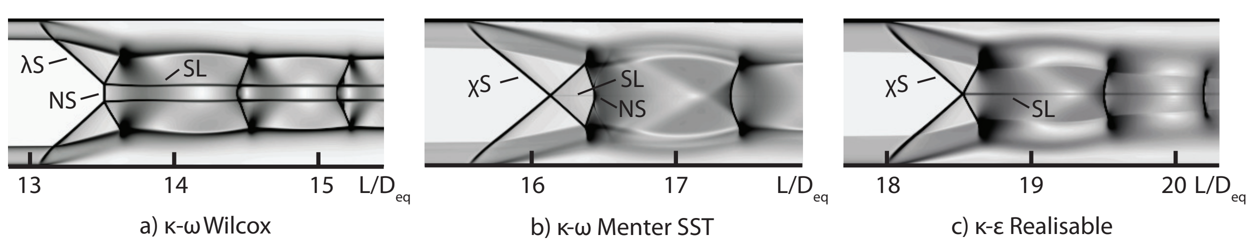

Figure 8. Close up of numerical schlieren at the corresponding first shock with different turbulence model.

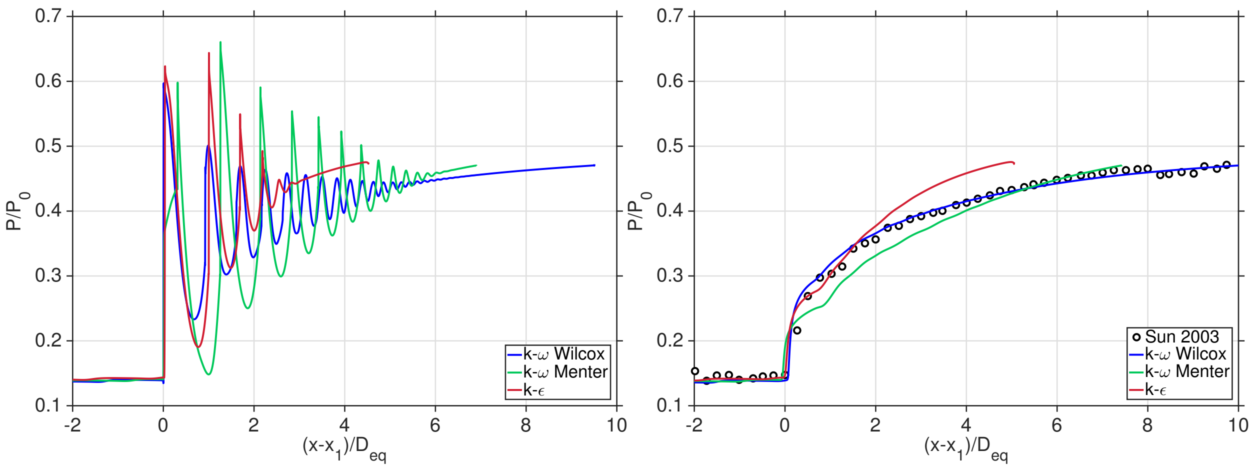

(a) (b)

Figure 9. Effect of turbulence model on the accuracy of the static pressure distribution at the duct centreline (a) and at the wall (b). The plots are shifted for common pressure rise and normalised to the equivalent hydraulic diameter.

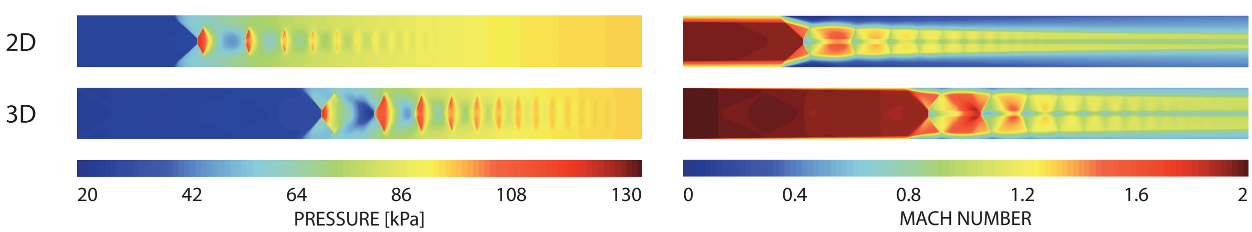

Figure 10. Comparison of pressure and Mach number contour in the 2D (upper) and 3D (lower) domains.

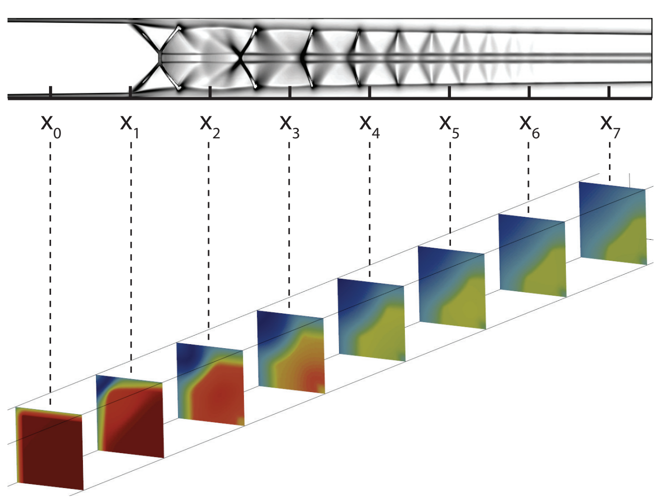

Figure 11. Numerical schlieren and Mach number contour at different axial locations.

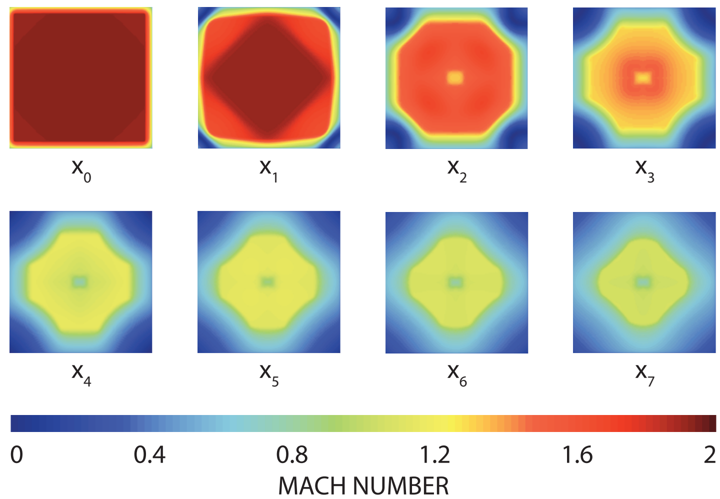

Figure 12. Mach number contour at different cross sections.

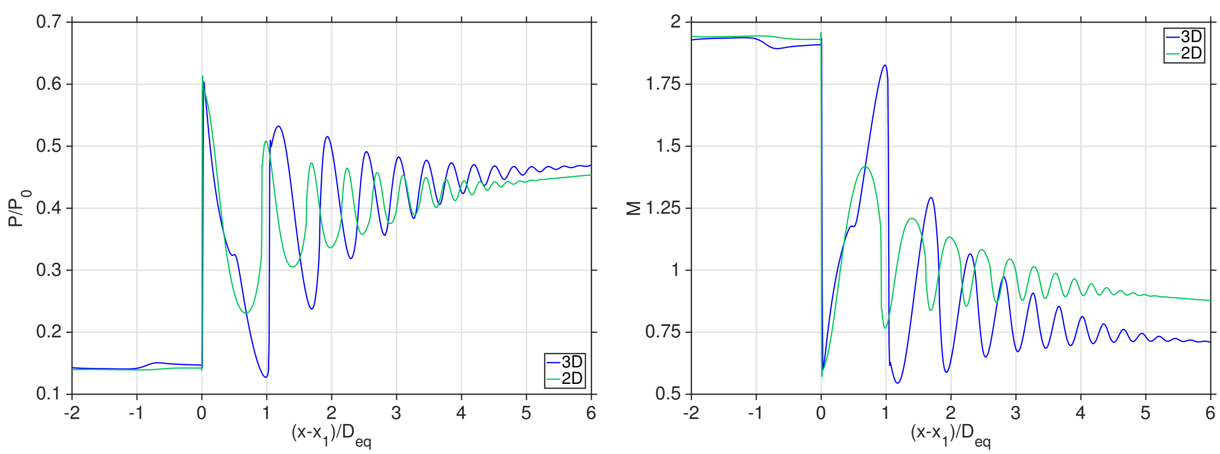

(a)

(b)

Figure 13. Centreline static pressure (a) and Mach number (b) distributions with 2D and 3D domain.